Added Stability Lobes in Machining Processes That Exhibit Periodic Time Variation, Part 1: An Analytical Solution

William T. Corpus[1]
Dept. of Mechanical Engineering,
University of Michigan,
Ann Arbor, MI 48109-215

William J. Endres
Dept. of Mechanical Engr.–Engr. Mechanics,
Michigan Technological University,
Houghton, MI 49931-1295

An added family of stability lobes, which exists in addition to the traditional stability lobes, has been identified for the case of periodically time varying systems. An analytical solution of arbitrary order is presented that identifies and locates multiple added lobes. The stability limit solution is first derived for zero damping where a final closed-form symbolic result can be realized up to second order. The un-damped solution provides a mathematical description of the added lobes' locations along the speed axis, an added-lobe numbering convention, and the asymptotes for the damped case. The derivation for the damped case permits a final closed-form symbolic result for first-order only; the second-order solution requires numerical evaluation. The easily computed analytical solution is shown to agree well with the results of the computationally intensive numerical simulation approach. An increase in solution order improves the agreement with numerical simulation; but, more importantly, it allows equivalently more added lobes to be predicted, including the second added lobe that cuts into the speed regime of the traditional high-speed stability peak. [DOI: 10.1115/1.1765137]

Introduction

It is well known that when increasing spindle speed to increase productivity the machining stability limit undergoes repeated increases and decreases. These increases and decreases result in peaks in the stability limit at well understood speeds—those where the dominant modal frequency is an integer multiple of the tooth frequency. Machining in the speed range around the two highest speed peaks is often referred to as *high-speed machining* [1]. Beyond the final highest-speed peak, the stability limit is understood to increase indefinitely with a further increase in speed. Operating at spindle speeds above about 1.5 times the dominant modal frequency is referred to here as *ultrahigh-speed machining*.

Research has led to a good understanding of the machining stability problem from a traditional system feedback perspective [2], a frequency-domain perspective [3–5] as well as an energy perspective [6–8], and the root-locus approach [9]. The fundamental nature of machining stability is well understood for cases in which each tooth is in contact with the workpiece at all times and the nominal machining force is constant over time.

During intermittent machining, each tooth periodically enters and exits the cut due to process kinematics and/or workpiece geometry. Stability of intermittent machining processes is also presumed to be well understood based on an evolution of studies focused on industrially used processes, in particular milling processes [5,6,10–12]. A goal of this work is to better understand the effect on stability of a periodically time varying process force, which often involves intermittency.

An added set of stability lobes is found to exist for periodic process loading, in both intermittent and continuous machining. In parallel with and independent of the research reported here, others have also discovered this phenomenon, most referring to it as "lobe splitting." In the present work, a one-dimensional orthogonal process is employed to facilitate an understanding of the basic effects of intermittency and time variation through simulation and physical experiments.

Davies et al. [14,15] observed the added lobes in low-immersion end milling where there exist substantial periods of free vibration (no engagement of any teeth). Based on time finite elements, Bayly et al. [16] provide a solution for interrupted turning, which had been noted by Davies et al. to be a good representation of low-immersion milling. These works, focusing on low immersions (e.g., up to 10%), show good agreement between the analytical solutions and numerical simulations. Insperger and Stépán [17] predict the ultrahigh-speed added lobe—as referred to here—which begins at tooth frequencies that are twice the natural frequency. Their work differs from the others in that it applies in the absence of free vibration. The first presentation resulting from our effort [18] is in agreement with those works; a primary difference lies in the generalization of the study/analysis here:

- it observes/predicts multiple added lobes for arbitrary levels of immersion, including cases where no periods of free vibration exist, and
- it considers/allows-for arbitrary overlap factor, including zero overlap.

Part 1 of this paper presents an analytical solution that locates the added lobes at only a fraction of the computational burden of numerical simulation and gives greater insight to the problem. Part 2 then provides a physical experimental study across a range of immersion levels that not only confirms the existence of the added lobes but also shows good agreement with the solution. It also employs the analysis of Part 1 to demonstrate the effects of overlap factor, multi-tooth cutting, and structural damping.

Setting up the Problem

The Equation of Motion. A single-degree-of-freedom machine-tool system under orthogonal cutting conditions, with the displacement coordinate q, can be represented as

$$m\ddot{q}(t)+c\dot{q}(t)+kq(t)=-u_T\cos\psi_r wh(t), \qquad (1)$$

[1]Now with Delphi Research Labs, Shelby Twp. MI, william.t.corpus@delphi.com

Contributed by the Manufacturing Engineering Division for publication in the JOURNAL OF MANUFACTURING SCIENCE AND ENGINEERING. Manuscript received Oct. 2002; Revised Dec. 2003. Associate Editor: Dong-Woo Cho.

where u_T is the specific thrust energy, ψ_r is the lead angle, w is the width of cut and $h(t)$ is the dynamic uncut chip thickness. If it is assumed, with no loss of generality, that the coordinate q lies in the tool feed direction, the uncut chip thickness is

$$h(t) = [q(t) - \mu q(t - T_t) + f_t]\cos\psi_r,$$

where f_t is the feed per tooth in the q direction and T_t is the tooth period and, likewise, the regenerative delay. The parameter μ is the overlap factor that accounts for the level of regeneration. It is usually assumed that $0 \leqslant \mu \leqslant 1$, though it has been shown to take on other values [19].

Accumulating all specific energy and directional terms into a single process gain, specifically

$$K_p = -u_T \cos^2 \psi_r,$$

Equation (1) reduces to

$$m\ddot{q} + c\dot{q} + kq = K_p w[q(t) - \mu q(t - T_t) + f_t], \tag{2}$$

where the explicit dependence on time in the left-hand side is dropped for convenience. When periodic time variation exists in the process force as it often does, it is incorporated into the process gain so that K_p becomes $K_p(t)$. It is convenient here to define the process gain in terms of its time-invariant part K_{pti} and its time varying part $K_{ptv}(t)$ as

$$K_p(t) = K_{pti} \cdot K_{ptv}(t) = -u_T \cos^2 \psi_r \cdot K_{ptv}(t). \tag{3}$$

The intermittency of machining is introduced within $K_p(t)$ as a switching function, $g(t)$ [5,20]. It is equal to unity while cutting and zero otherwise, and its period is the tooth period. In milling, the sources of time variation include both the switching function and the process (tooth-sweep) kinematics. For intermittent orthogonal tube-end turning/boring considered here, the kinematics are simple by design so that the only source of time variation is $g(t)$. Hence, for simplicity $K_{ptv}(t)$ is replaced by $g(t)$.

Others, having considered milling processes, have used "immersion" to quantify the extent of tooth engagement. Here, duty cycle is used instead; it is loosely described as the percentage of the machining (spindle) period spent cutting. It can be defined from the perspective of either a single tooth or the spindle. The tooth duty cycle, $\mathcal{D}_t$, is defined as the percentage of the spindle period for which *an individual tooth* is engaged in the cut. Like the traditional definition of a duty cycle, the tooth duty cycle can range from zero to unity. The spindle duty cycle, $\mathcal{D}_s$, equals $\mathcal{D}_t$ for the case of single-tooth machining. More generally, assuming evenly spaced teeth, $\mathcal{D}_s = N_t \mathcal{D}_t$, where N_t is the number of teeth. Clearly, the spindle duty cycle can assume values greater than unity, which provides for generalization to the multi-tooth case where there need not exist periods of free vibration.

Introducing Eq. (3) into Eq. (2), dividing through by the mass, regrouping terms, and dropping the feed term (f_t) that does not affect stability, the equation of motion to be studied results as

$$\ddot{q} + 2\zeta\omega_n\dot{q} + \omega_n^2 q = \frac{K_{pti} w}{k}\omega_n^2 g(t)[q(t) - \mu q(t - T_t)], \tag{4}$$

where ω_n and ζ are the structural natural frequency and damping ratio, respectively. Single-tooth machining is assumed for the derivations here; extension to multi-tooth machining would be a fairly straightforward exercise though the results are less compact. Furthermore, the process force is treated as linear by linearizing the size-effect nonlinearity introduced by the specific energy as a first step in analyzing the added-lobe problem.

General Problem Characteristics. Exploratory numerical time-domain simulations were conducted to study the effects of process and structural parameters on the effects of intermittency and ultimately on the ultrahigh-speed added lobe that was identified. The machine-tool system is routinely implemented in a simulation package, such as Matlab. In addition to determining stability (growth or decay of the response to a disturbance), it was also desired to study the steady-state chatter frequency, which requires that a sufficient number of previous tooth passes (long-term process memory) be included [21].

A power-spectrum study indicates that chatter in the ultrahigh-speed added lobe occurs primarily at one-half the tooth frequency. Therefore, later references to the chatter frequency in the added lobes imply one-half the tooth frequency. As expected, the tooth frequency and its harmonics dominate during stable machining. The one-half tooth frequency and the tooth frequency are both present along the ultrahigh-speed added lobe boundary.

The effects of structural stiffness, mass, natural frequency and specific energy are consistent with those that have been observed in traditional stability analyses for intermittent and continuous machining. As such, the limiting width of cut w_{lim} may be presented as a non-dimensional stability limit $K_{pti} w_{lim}/k$, the leading term on the right-hand side of Eq. (4). Given that and the fact that the speed axis can be presented as the normalized tooth frequency $\Omega_t = \omega_t/\omega_n$, there is no need to specify values for many of the system parameters, such as specific energy (i.e., K_{pti}), natural frequency, and structural stiffness k. The only parameters that must be quantified are damping ratio, ζ, and overlap factor, μ, which are set to 0.05 and 1, respectively, unless noted otherwise; their effects will be studied in Part 2.

The Chatter Frequency and the Regenerative Delay Term. The results of the numerical simulations clearly demonstrate that the added-lobe chatter frequency is one-half the tooth frequency, ω_t. The Appendix further confirms this by providing an analytical/mathematical argument that is familiar to the dynamics community. The presented argument is the foundation of others' observations [15,16] that the flip bifurcation leading to the added-lobe instability corresponds to a real eigenvalue passing through -1 to the outside of the unit circle. This is in contrast to the Hopf bifurcation instability that leads to the traditional stability lobes.

The response on the added-lobe boundary includes only integer multiples (harmonics) of one-half the tooth frequency. As a result, all harmonics of the current tooth pass displacement $q(t)$ and the previous-pass displacement $q(t - T_t)$ are either in phase (even harmonics) or 180° out of phase (odd harmonics). Therefore, the $q(t)$ and $q(t - T_t)$ terms may be combined by replacing $\mu q(t - T_t)$ in Eq. (4) with $\pm\mu q(t)$ (+ for even harmonics, − for odd harmonics) to obtain

$$\ddot{q} + 2\zeta\omega_n\dot{q} + \omega_n^2 q = \frac{K_{pti} w}{k}\omega_n^2 g(t)[(1 \pm \mu)q(t)]. \tag{5}$$

The analysis for arbitrary overlap factor is possible, but quickly becomes very complicated. To simplify matters in the derivation here, only the simpler case of unity overlap is considered. This simplification does not introduce a limitation as will be shown in Part 2 of this work.

Setting the overlap factor to unity, $q(t)$ and $\mu q(t - T_t)$ cancel for all their components at the tooth frequency and its harmonics, i.e., for even harmonics of $\omega_t/2$, $(1 \pm \mu) \rightarrow (1 - 1) = 0$ in Eq. (5). On the other hand, $q(t)$ and $\mu q(t - T_t)$ add for all their components at one-half the tooth frequency and its odd harmonics, i.e., $(1 \pm \mu) \rightarrow (1 + 1) = 2$ in Eq. (5). As a result, Eq. (5) becomes

$$\ddot{q} + 2\zeta\omega_n\dot{q} + \omega_n^2 q = \frac{K_{pti} w}{k}\omega_n^2 g(t)[2q(t)],$$

or

$$\ddot{q} + 2\zeta\omega_n\dot{q} + \omega_n^2\left(1 - 2\frac{K_{pti} w}{k}g(t)\right)q = 0, \tag{6}$$

where $q(t)$ includes only odd harmonics of one-half the tooth frequency.

The Periodically Time Varying Process Gain. The periodic time variation is addressed by approximating the process gain, specifically $K_{ptv}(t)$, with its Fourier series expansion. In this case, since $K_{ptv}(t)$ is simply $g(t)$, the problem is simplified; however, the methods presented here apply to any form of $K_{ptv}(t)$ that is T_t-periodic. Since the derivation is constrained to a single tooth, the spindle and tooth duty cycles are identical and are simply referred to as the duty cycle $\mathcal{D}$.

Without loss of generality, if $g(t)$ is considered to be time-referenced so that its square pulse is centered at the origin, $g(t)$ is an even function. This simplifies its Fourier series expansion to include only cosine terms. Expanding $g(t)$ and substituting into Eq. (6) results in

$$\ddot{q}+2\zeta\omega_n\dot{q}+\omega_n^2\left(1-2\mathcal{D}\frac{K_{pti}w}{k}-\frac{4}{\pi}\frac{K_{pti}w}{k}\sum_{l=1}^{\infty}\frac{(-1)^{l+1}}{l}\sin(l\pi\mathcal{D})\cos(2l\omega_1 t)\right)q=0, \tag{7}$$

which is in the form of Hill's equation with period π/ω_1 or, equivalently, $2\pi/\omega_t$. Equation (7) may be rewritten as

$$\ddot{q}+2\zeta\omega_n\dot{q}+\left(\delta+2\varepsilon\sum_{l=1}^{\infty}\beta_l\cos(2l\omega_1 t)\right)q=0, \tag{8}$$

where

$$\beta_l=\frac{(-1)^{l+1}}{l}\sin(l\mathcal{D}\pi),\quad \varepsilon=\omega_n^2\left(\frac{2}{\pi}\frac{K_{pti}w}{k}\right)$$

and

$$\delta=\omega_n^2\left(1-2\mathcal{D}\frac{K_{pti}w}{k}\right)=\omega_n^2-\pi\mathcal{D}\varepsilon.$$

To summarize thus far, the Hill's equation form has been achieved by (1) linearizing the process force, (2) mathematically confirming the existence of one-half the tooth frequency on the stability boundary (Appendix), (3) setting, without limitation, overlap factor to unity, and (4) approximating the periodicity with a Fourier series expansion.

The Assumed Response. As noted earlier, the assumed form of the response that need be considered for $\mu=1$ includes only terms at odd multiples of one-half the tooth frequency. Therefore, the assumed response is written as

$$q(t)=\sum_{i=1}^{\infty}[a_{2i-1}\sin((2i-1)\omega_1 t)+b_{2i-1}\cos((2i-1)\omega_1 t)], \tag{9}$$

where $\omega_1=\omega_t/2$. Substituting Eq. (9) into Eq. (8) results in

$$\begin{aligned}&-\omega_1^2\sum_{i=1}^{\infty}(2i-1)^2[a_{2i-1}\sin((2i-1)\omega_1 t)+b_{2i-1}\cos((2i-1)\omega_1 t)]+2\zeta\omega_n\omega_1\sum_{i=1}^{\infty}(2i-1)[a_{2i-1}\cos((2i-1)\omega_1 t)\\&-b_{2i-1}\sin((2i-1)\omega_1 t)]+\left(\delta+2\varepsilon\sum_{l=1}^{\infty}\beta_l\cos(2l\omega_1 t)\right)\times\sum_{i=1}^{\infty}[a_{2i-1}\sin((2i-1)\omega_1 t)+b_{1i-1}\cos((2i-1)\omega_1 t)]\\&=0.\end{aligned}$$

This expands to

$$\begin{aligned}&-\omega_1^2[a_1\sin\omega_1 t+b_1\cos\omega_1 t]-(3\omega_1)^2[a_3\sin 3\omega_1 t+b_3\cos 3\omega_1 t]-(5\omega_1)^2[a_5\sin 5\omega_1 t+b_5\cos 5\omega_1 t]-\ldots\\&+2\zeta\omega_n\omega_1[a_1\cos\omega_1 t-b_1\sin\omega_1 t]+3(2\zeta\omega_n\omega_1)[a_3\cos 3\omega_1 t-b_3\sin 3\omega_1 t]+5(2\zeta\omega_n\omega_1)[a_5\cos 5\omega_1 t-b_5\sin 5\omega_1 t]+\ldots\\&+\delta[a_1\sin\omega_1 t+b_1\cos\omega_1 t]+\delta[a_3\sin 3\omega_1 t+b_3\cos 3\omega_1 t]+\delta[a_5\sin 5\omega_1 t+b_5\cos 5\omega_1 t]+\ldots\\&+2\varepsilon\beta_1\cos(2\omega_1 t)[a_1\sin\omega_1 t+b_1\cos\omega_1 t+a_3\sin 3\omega_1 t+b_3\cos 3\omega_1 t+a_5\sin 5\omega_1 t+b_5\cos 5\omega_1 t+\ldots]\\&+2\varepsilon\beta_2\cos(4\omega_1 t)[a_1\sin\omega_1 t+b_1\cos\omega_1 t+a_3\sin 3\omega_1 t+b_3\cos 3\omega_1 t+a_5\sin 5\omega_1 t+b_5\cos 5\omega_1 t]+\ldots\\&+2\varepsilon\beta_3\cos(6\omega_1 t)[a_1\sin\omega_1 t+b_1\cos\omega_1 t+a_3\sin 3\omega_1 t+b_3\cos 3\omega_1 t+a_5\sin 5\omega_1 t+b_5\cos 5\omega_1 t]+\ldots\\&\vdots\\&=0.\end{aligned} \tag{10}$$

For the third-from-last block of terms in Eq. (10), multiplying the $\cos(2\omega_1 t)$ term through the bracketed summation of harmonics, and employing trigonometric identities, leads to

$$\begin{aligned}&\varepsilon\beta_1[a_1(\sin 3\omega_1 t-\sin\omega_1 t)+b_1(\cos 3\omega_1 t+\cos\omega_1 t)\\&+a_3(\sin 5\omega_1 t+\sin\omega_1 t)+b_3(\cos 5\omega_1 t+\cos\omega_1 t)\\&+a_5(\sin 7\omega_1 t+\sin 3\omega_1 t)+b_5(\cos 7\omega_1 t+\cos 3\omega_1 t)\\&+a_7(\sin 9\omega_1 t+\sin 5\omega_1 t)+b_7(\cos 9\omega_1 t+\cos 5\omega_1 t)\\&+\ldots].\end{aligned}$$

The same can be done for the final two blocks of terms in Eq. (10), i.e., multiplying through $\cos(4\omega_1 t)$ and $\cos(6\omega_1 t)$, so that the coefficients of $\sin(n\omega_1 t)$ and $\cos(n\omega_1 t)$, n odd, can be grouped. A pattern becomes evident that allows Eq. (10) to be expressed in matrix form as

$$\{H\}^T[A]\{C\}=0, \tag{11}$$

where

$$\{H\}=\{\sin\omega_1 t\ \ \cos\omega_1 t\ \ \sin 3\omega_1 t\ \ \cos 3\omega_1 t\ \ \sin 5\omega_1 t\ \ \cos 5\omega_1 t\ \ \cdots\}^T,$$

$$\{C\}=\{a_1\ \ b_1\ \ a_3\ \ b_3\ \ a_5\ \ b_5\ \ \cdots\}^T,$$

and

$$[A]=\begin{bmatrix}
\delta-\omega_1^2-\varepsilon\beta_1 & -2\zeta\omega_n\omega_1 & \varepsilon(\beta_1-\beta_2) & 0 & & \varepsilon(\beta_2-\beta_3) & 0 & \cdots \\
2\zeta\omega_n\omega_1 & \delta-\omega_1^2+\varepsilon\beta_1 & 0 & \varepsilon(\beta_1+\beta_2) & & 0 & \varepsilon(\beta_2+\beta_3) & 0 \\
\varepsilon(\beta_1-\beta_2) & 0 & \delta-(3\omega_1)^2-\varepsilon\beta_3 & -3(2\zeta\omega_n\omega_1) & & \varepsilon(\beta_1-\beta_4) & 0 & \varepsilon(\beta_2-\beta_5) \\
0 & \varepsilon(\beta_1+\beta_2) & 3(2\zeta\omega_n\omega_1) & \delta-(3\omega_1)^2+\varepsilon\beta_3 & \cdots\ \cdots & 0 & \varepsilon(\beta_1+\beta_4) & 0 \\
\varepsilon(\beta_2-\beta_3) & 0 & \varepsilon(\beta_1-\beta_4) & 0 & & \delta-(5\omega_1)^2-\varepsilon\beta_5 & -5(2\zeta\omega_n\omega_1) & \varepsilon(\beta_1-\beta_6) \\
0 & \varepsilon(\beta_2+\beta_3) & 0 & \varepsilon(\beta_1+\beta_4) & & 5(2\zeta\omega_n\omega_1) & \delta-(5\omega_1)^2+\varepsilon\beta_5 & 0 \\
\vdots & 0 & \varepsilon(\beta_2-\beta_5) & 0 & & \varepsilon(\beta_1-\beta_6) & 0 & \ddots
\end{bmatrix}. \tag{12}$$

Now, since $\{H\}$ cannot be zero for all time, and $\{C\}=\{0\}$ would be a trivial solution, the solution to Eq. (11) requires that the determinant of $[A]$ be zero. Since an exact solution to an infinite determinant is not possible, the determinant is truncated to $2O\times 2O$ where O is the order of the solution. This results in O added stability lobes being identified along the speed axis, not just the single ultrahigh-speed added lobe that was studied in the previous works [18,22].

If arbitrary overlap factor were considered, the $2K_{pti}$ term starting in Eq. (6) would be simply replaced by $(1+(-1)^{n+1}\mu)K_{pti}$, while the complication would come from appending to the above equations a_n, b_n, $\sin(n\omega_1 t)$, and $\cos(n\omega_1 t)$, *n even*. Ultimately, the "even" and "odd" terms can be decoupled in $[A]$ with the odd terms being of interest; this allows the simplified $\mu=1$ presentation thus far to bypass the need for the added mathematical notation.

The Un-Damped Solution

The un-damped case is an extreme scenario that typically will not exist in practice. However, the zero-damping solution does provide an asymptotic view of the added stability boundaries. Studying the boundary asymptotes is enlightening in that it solidifies a pattern to the multiple added lobes in terms of their positioning along the speed axis, just as there is a mathematical logic to the positioning of the traditional stability lobes along that axis.

For the case of zero damping the $\sin(n\omega_1 t)$ and $\cos(n\omega_1 t)$ terms in Eq. (11) decouple, which results in two determinants, each being of dimension equal to the order of the problem, O, rather than $2O$, which greatly simplifies matters. When this is done, Eq. (11) can be rewritten as

$$\{H_s\}^T[A_s]\{C_s\}+\{H_c\}^T[A_c]\{C_c\}=0,$$

where

$$\{H_s\}=\begin{Bmatrix}\sin\omega_1 t\\ \sin 3\omega_1 t\\ \sin 5\omega_1 t\\ \vdots\end{Bmatrix},\quad \{H_c\}=\begin{Bmatrix}\cos\omega_1 t\\ \cos 3\omega_1 t\\ \cos 5\omega_1 t\\ \vdots\end{Bmatrix},$$

$$\{C_s\}=\begin{Bmatrix}a_1\\ a_3\\ a_5\\ \vdots\end{Bmatrix},\quad \{C_c\}=\begin{Bmatrix}b_1\\ b_3\\ b_5\\ \vdots\end{Bmatrix},$$

$$[A_s]=\begin{bmatrix}
\delta-\omega_1^2-\varepsilon\beta_1 & \varepsilon(\beta_1-\beta_2) & \varepsilon(\beta_2-\beta_3) & \varepsilon(\beta_3-\beta_4) & \cdots \\
\varepsilon(\beta_1-\beta_2) & \delta-(3\omega_1)^2-\varepsilon\beta_3 & \varepsilon(\beta_1-\beta_4) & \varepsilon(\beta_1-\beta_5) & \\
\varepsilon(\beta_2-\beta_3) & \varepsilon(\beta_1-\beta_4) & \delta-(5\omega_1)^2-\varepsilon\beta_5 & \varepsilon(\beta_1-\beta_6) & \\
\varepsilon(\beta_3-\beta_4) & \varepsilon(\beta_1-\beta_5) & \varepsilon(\beta_1-\beta_6) & \delta-(7\omega_1)^2-\varepsilon\beta_7 & \\
\vdots & & & & \ddots
\end{bmatrix},$$

and

$$[A_c]=\begin{bmatrix}
\delta-\omega_1^2+\varepsilon\beta_1 & \varepsilon(\beta_1+\beta_2) & \varepsilon(\beta_2+\beta_3) & \varepsilon(\beta_3+\beta_4) & \cdots \\
\varepsilon(\beta_1+\beta_2) & \delta-(3\omega_1)^2+\varepsilon\beta_3 & \varepsilon(\beta_1+\beta_4) & \varepsilon(\beta_1+\beta_5) & \\
\varepsilon(\beta_2+\beta_3) & \varepsilon(\beta_1+\beta_4) & \delta-(5\omega_1)^2+\varepsilon\beta_5 & \varepsilon(\beta_1+\beta_6) & \\
\varepsilon(\beta_3+\beta_4) & \varepsilon(\beta_1+\beta_5) & \varepsilon(\beta_1+\beta_6) & \delta-(7\omega_1)^2+\varepsilon\beta_7 & \\
\vdots & & & & \ddots
\end{bmatrix}.$$

Like in the damped case, the solution where $\{C_s\}$ and $\{C_c\}$ are zero is a trivial one, and since $\{H_s\}$ and $\{H_c\}$ are harmonic functions of time, the only *nontrivial* solution that holds *for all time* corresponds to the determinants of $[A_s]$ *and* $[A_c]$ being zero.

An Added-Lobe Numbering Convention. Locating the added lobes along the speed axis involves determining the speeds that correspond to a zero width of cut. Setting the width of cut to zero makes ε equal to zero and δ equal to ω_n^2. Substituting these into $[A_s]$ and $[A_c]$ shows that the two become equal, resulting in a single equation

$$\begin{vmatrix} \omega_n^2-\omega_1^2 & 0 & 0 & \cdots \\ 0 & \omega_n^2-(3\omega_1)^2 & 0 & \\ 0 & 0 & \ddots & \\ \vdots & & & \omega_n^2-((2i-1)\omega_1)^2 \end{vmatrix}=0. \tag{13}$$

The determinant in this case is simply the product of the entries on the diagonal, which is equal to zero if any one of the diagonal terms is zero, i.e., if

$$\left(\frac{\omega_t}{\omega_n}\right)^2=\left(\frac{2}{2i-1}\right)^2 \Rightarrow \frac{\omega_t}{\omega_n}=\frac{2}{2i-1},$$
$$i=1,2,3\rightarrow 2i-1=1,3,5,\ldots. \tag{14}$$

Equation (14) introduces a lobe numbering scheme where the ultrahigh-speed added lobe is numbered "1/2"—the value of ω_n/ω_t (not ω_t/ω_n) to which the two un-damped added-lobe boundaries converge to one another at $w=0$. Following this convention, the lower-speed added lobes that are subsequently illuminated with each increase in order O are numbered 3/2, 5/2 and so on. Recall that the traditional lobes are numbered 0, 1, 2, . . . as speed *decreases*, where this number is the integer portion of the ratio ω_n/ω_c, ω_c being the chatter frequency. As such, the two numbering schemes are analogous.

Zero-Damping Added-Lobe Solutions. As noted above, obtaining a solution requires truncation to the order O. Furthermore, since this case of zero damping permits the single $2O\times 2O$ determinant to be split into two $O\times O$ determinants, it is possible to derive symbolically the solution for the first two added lobes (1/2 and 3/2; i.e., $O=2$).

Noting that $[A_s]$ and $[A_c]$ are of the same form, differing only by a flip in sign on many of the terms, they may be written as

$$\begin{bmatrix} \delta-\omega_1^2\mp\varepsilon\beta_1 & \varepsilon(\beta_1\mp\beta_2) \\ \varepsilon(\beta_1\mp\beta_2) & \delta-(3\omega_1)^2\mp\varepsilon\beta_3 \end{bmatrix},$$

where using the top of the $\mp$ signs gives the result for $[A_s]$. Substituting the expressions for δ and ε and dividing through by ω_n^2, the problem becomes

$$\begin{vmatrix} 1-\Omega_t^2-\frac{2}{\pi}\frac{K_{pti}w}{k}(\pi\mathcal{D}\pm\beta_1) & \frac{2}{\pi}\frac{K_{pti}w}{k}(\beta_1\mp\beta_2) \\ \frac{2}{\pi}\frac{K_{pti}w}{k}(\beta_1\mp\beta_2) & 1-(3\Omega_t)^2-\frac{2}{\pi}\frac{K_{pti}w}{k}(\pi\mathcal{D}\pm\beta_3) \end{vmatrix}=0,$$

where $\Omega_t=\omega_t/\omega_n$ is the normalized tooth frequency.

Writing out the determinant produces a quadratic in w, which yields two solutions, w_1 and w_3, for each case (of the $\pm$ and $\mp$ signs). In other words, there exist two pairs of solutions, $w_{1_{a,b}}$ and $w_{3_{a,b}}$, where one pair corresponds to the "+" on the square-root term in the quadratic formula, and the other pair corresponds to the "−" on that term. In other words, the subscripts "1" and "3" refer to lobes 1/2 and 3/2, and the subscripts "a" and "b" refer to the two boundaries (left and right) that together form the lobe. The result is

$$w_{1_{a,b},3_{a,b}}=\frac{\rho_{a,b}\pm\sqrt{\rho_{a,b}^2-4\kappa_{a,b}(1-\Omega_t^2)^2}}{\frac{4\kappa_{a,b}}{\pi}\frac{K_{pti}}{k}}, \tag{15}$$

where

$$\rho_{a,b}=(\Omega_t^2-1)[2\pi\mathcal{D}\pm(\beta_1+\beta_3)^2]$$

and

$$\kappa_{a,b}=(\pi\mathcal{D}\pm\beta_1)(\pi\mathcal{D}\pm\beta_3)-(\beta_1\mp\beta_2)^2.$$

The 1/2 and 3/2 lobes for $\mathcal{D}=1/2$ are graphed in Fig. 1, displayed as the nondimensional stability limit $K_{pti}w_{lim}/k$.[2]

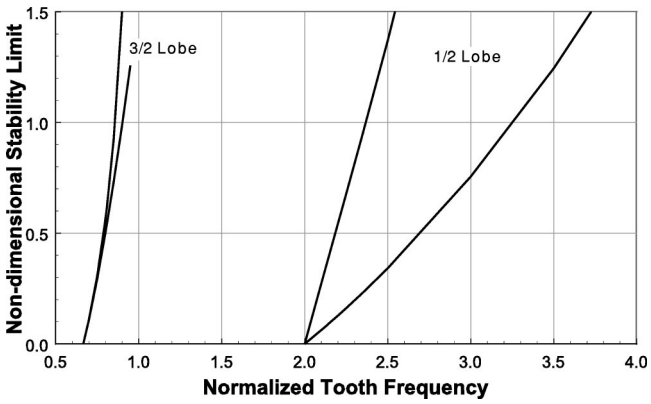

Fig. 1 Undamped second-order stability solutions showing the 1/2 and 3/2 lobes for a one-half duty cycle

The Damped Solution

When damping is not zero, the original matrix $[A]$ of Eq. (12) must be evaluated. The first consequence of non-zero damping is that when w is set equal to zero (i.e., $\varepsilon=0$ and $\delta=\omega_n^2$),

[2]Numerical simulation shows the ultra-high speed added lobe to become more pronounced for lower duty cycles, and gradually less pronounced for duty cycles higher than one-half. In other words, the one-half duty cycle used to visualize the analytical results (in the figures) is a middle-of-the-road representative value, not one that accentuates the added lobe.

$$[A]=\begin{bmatrix} \omega_n^2-\omega_1^2 & -2\zeta\omega_n\omega_1 & 0 & 0 & \cdots & \cdots \\ 2\zeta\omega_n\omega_1 & \omega_n^2-\omega_1^2 & 0 & 0 & \cdots & \cdots \\ 0 & 0 & \omega_n^2-(3\omega_1)^2 & -3(2\zeta\omega_n\omega_1) & 0 & 0 \\ 0 & 0 & 3(2\zeta\omega_n\omega_1) & \omega_n^2-(3\omega_1)^2 & 0 & 0 \\ \vdots & \vdots & 0 & 0 & \ddots & \ddots \\ \vdots & \vdots & 0 & 0 & \ddots & \ddots \end{bmatrix}.$$

This matrix is no longer diagonal as it was in Eq. (13) for the un-damped case. However, being block-wise diagonal, the solutions for ω_t/ω_n occur in pairs that result from setting each 2×2 sub-determinant equal to zero. It can be shown that these solutions for ω_t/ω_n are complex conjugate pairs for all non-zero damping ratios less than unity; damping ratios of unity and above are not seen in practice and, hence, are not of interest here. Since only real-valued solutions for tooth frequency are physically sensible, this means that the stability limit can never actually be zero on these added lobes when there exists positive (and less than critical) damping. This makes sense.

For the first-order case, truncating Eq. (12) to a 2×2 matrix and equating its determinant to zero yields

$$\begin{vmatrix} \delta-\omega_1^2-\varepsilon\beta_1 & -2\zeta\omega_n\omega_1 \\ 2\zeta\omega_n\omega_{1_1} & \delta-\omega_1^2+\varepsilon\beta_1 \end{vmatrix}=0.$$

Substituting the expressions for δ and ε, replacing ω_1 with $\omega_t/2$, dividing through by ω_n^2 and multiplying by 4 yields

$$\begin{vmatrix} 4-\Omega_t^2-8(\pi\mathcal{D}+\beta_1)\dfrac{1}{\pi}\dfrac{K_{pti}w}{k} & -4\zeta\Omega_t \\ 4\zeta\Omega_t & 4-\Omega_t^2-8(\pi\mathcal{D}-\beta_1)\dfrac{1}{\pi}\dfrac{K_{pti}w}{k} \end{vmatrix}=0. \tag{16}$$

Solving the resulting quadratic in w, a pair of solutions results as

$$w_{lim}=\frac{\pi\mathcal{D}(\Omega_t^2-4)\pm\sqrt{\beta_1^2[\Omega_t^4-8\Omega_t^2+16(1+\Omega_t^2\zeta^2)]-(4\pi\mathcal{D}\Omega_t\zeta)^2}}{\dfrac{8}{\pi}\dfrac{K_{pti}}{k}(\beta_1^2-\pi^2\mathcal{D}^2)}. \tag{17}$$

The second consequence of non-zero damping is that even the second-order solution requires evaluating a 4×4 determinant. While this is no problem with a numerical approach, it is not suited to a clear symbolic derivation to a final closed form.

The computational results for the one-half lobe are shown in Fig. 2, which demonstrate very good agreement between the second-order solution and the solution found through numerical time-domain simulations. The figure also confirms that the intuition-based first-order approach of Corpus [18] and the first-order solution found above are identical, as may be expected. This figure validates the objective of this effort—to provide the same results as a numerical simulation through an analytical solution that can be computed in only a small fraction of the time associated with the numerical simulation approach. Part 2 proceeds to validate the physical existence of the added lobes as well as the quantitative accuracy of the numerical and analytical results through a physical experiment.

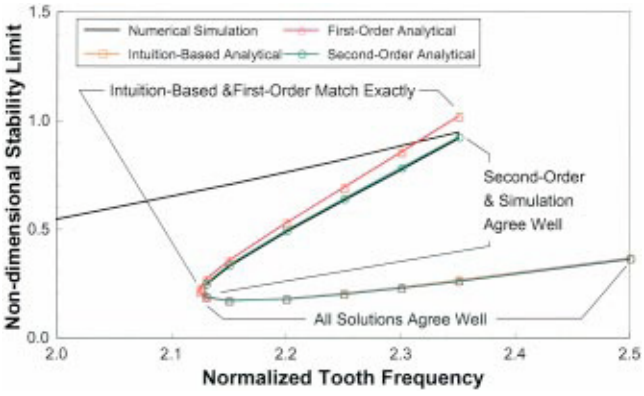

Fig. 2 Comparison of solution approaches for the 1/2 lobe for a one-half duty cycle

From the perspective of practical applications, in light of the typical uncertainties in structural dynamic parameters and specific energy, computing the second- or third-order solution and the added accuracy it provides may not yield any significant advantage over the first-order solution. However, the second-order solution is needed to predict the 3/2 lobe, which is likely to have practical significance since it falls within the same speed regime as does the traditional high-speed (0-1) peak—the usual target for increased productivity in high-speed machining. From the perspective of being able to predict more added lobes, a third-order solution and the 5/2 lobe that it would predict is probably not warranted since the traditional 1–2 peak that it may affect is usually too narrow to operate within anyway.

Conclusions

The locations of the added lobes along the speed axis are shown to occur in a mathematically definable pattern that is highlighted by the zero-damping solution. The first-order damped solution accurately predicts, relative to the more time consuming numerical simulation, the lower/right-hand stability boundary and exhibits roughly 10% error at the upper/left-hand boundary. This is reasonably accurate considering the simplicity of the closed-form solution that is possible. The second-order solution is highly accurate at both boundaries when compared to the numerical simulation results.

Acknowledgments

The authors wish to gratefully acknowledge the partial financial support of Dr. Corpus' continuing education that was provided by his former employer, EDS.

Appendix

Since all other aspects of the problem are linear (or linearized) and the chatter nonlinearity is not present for sufficiently small disturbances from equilibrium, such as at the stability boundary, superposition may be employed to obtain a solution *for the response* to such a disturbance. As such, Eq. (4) (with f_t term) can be broken into the following equations:

$$\ddot{q}+2\zeta\omega_n\dot{q}+\omega_n^2 q=\frac{K_{pti}w}{k}\omega_n^2 g(t)\cdot f_t, \tag{18}$$

$$\ddot{q}+2\zeta\omega_n\dot{q}+\omega_n^2 q=\frac{K_{pti}w}{k}\omega_n^2 g(t)\cdot q(t), \tag{19}$$

and

$$\ddot{q}+2\zeta\omega_n\dot{q}+\omega_n^2 q=-\frac{K_{pti}w}{k}\omega_n^2 g(t)\cdot \mu q(t-T_t). \tag{20}$$

Since $g(t)$ is periodic, the solution to Eq. (18) is that of a forced vibration at the tooth frequency and its harmonics; therefore, it does not affect the stability problem, which agrees with the numerical simulation findings of Corpus [18]. Equation (20) is identical to Eq. (19), except that it is shifted in time by the tooth period and multiplied by negative μ. The periodic solution to Eq. (20) will therefore exhibit the same period as the solution to Eq. (19). If this common period is assumed to be an integer multiple of the time delay in Eq. (20) (the tooth period T_t), then Eq. (20) and Eq. (19) may be combined (added) in an expansion, resulting in the following homogeneous equation:

$$\ddot{q}(t)+2\zeta\omega_n\dot{q}(t)+\omega_n^2\left[1-(1-\mu)\frac{K_{pti}w}{k}g(t)\right]q(t)=0. \tag{21}$$

It will be confirmed below that the above assumption is valid.

Following Nayfeh and Mook [23], since Eq. (21) is linear, it can be written as a linear combination of two linearily independent solutions such that

$$q(t)=c_1 q_1(t)+c_2 q_2(t), \tag{22}$$

where c_1 and c_2 are constants and $q_1(t)$ and $q_2(t)$ is termed the *fundamental set of solutions*. The fundamental set of solutions for a system of this type is of the form

$$q_i(t)=\phi_i(t)e^{\rho_i t}, \tag{23}$$

where the coefficient $\phi_i(t)$ introduces the periodic time variation, and ρ_i, the characteristic exponent, is taken from (is a root of) the characteristic equation.

The bracketed coefficient of $q(t)$ in Eq. (21) varies in time with period T_t. Therefore, Eq. (21) may be rewritten after one tooth period[3]

$$\ddot{q}(t+T_t)+2\zeta\omega_n\dot{q}(t+T_t)+\omega_n^2\left[1-(1-\mu)\frac{K_{pti}w}{k}g(t)\right]q(t+T_t)=0. \tag{24}$$

The bracketed term is unchanged since the equation has been shifted in time by its period (that of $g(t)$). The solution to Eq. (24) is identical in form to Eq. (22), namely

$$q(t+T_t)=c_1 q_1(t+T_t)+c_2 q_2(t+T_t).$$

Furthermore, since Eq. (24) is identical to Eq. (21) having been shifted by T_t, the two equations differ only in their initial conditions. Because Eqs. (21) and (24) are the same equation, if $q_1(t)$ and $q_2(t)$ is a fundamental set of solutions to Eq. (21), then $q_1(t+T_t)$ and $q_2(t+T_t)$ is as well.

From Eq. (22), it is determined that $q_1(t+T_t)$ and $q_2(t+T_t)$ can be written as a linear combination of $q_1(t)$ and $q_2(t)$ as

$$q_i(t+T_t)=\gamma_{i1}q_1(t)+\gamma_{i2}q_2(t), \quad i=1,2,$$

or in matrix format as

$$\{q(t+T_t)\}=[\Gamma]\{q(t)\}, \tag{25}$$

where $\{q(t)\}=\{q_1(t)\ q_2(t)\}^T$ and $[\Gamma]$ is a constant non-singular matrix. There then exists another fundamental set of solutions to Eq. (21), $v_1(t)$ and $v_2(t)$, such that

$$\{q(t)\}=[P]\{v(t)\}, \tag{26}$$

where $\{v(t)\}=\{v_1(t)\ v_2(t)\}^T$ and $[P]$ is a constant non-singular matrix. Substituting Eq. (26) into Eq. (25) and rearranging yields

$$\{v(t+T_t)\}=[\Lambda]\{v(t)\}, \tag{27}$$

where $[\Lambda]=[P]^{-1}[\Gamma][P]$.

The matrix $[\Lambda]$ is similar to $[\Gamma]$ and, hence, has the same eigenvalues. To simplify the form of $[\Lambda]$, the columns of $[P]$ are chosen as the normalized eigenvectors of $[\Gamma]$ such that

$$|[\Gamma]-\lambda[I]|=0, \tag{28}$$

where λ is an eigenvalue of $[\Gamma]$ and $[I]$ is the identity matrix. Assuming distinct roots of the characteristic equation that is represented by Eq. (28), the form of $[\Lambda]$ is

$$[\Lambda]=\begin{bmatrix}\lambda_1 & 0\\ 0 & \lambda_2\end{bmatrix}.$$

Equation (27) may then be expanded and rewritten as

$$v_i(t+T_t)=\lambda_i v_i(t), \quad i=1,2.$$

Furthermore,

$$\begin{aligned} v_i(t+2T_t)&=\lambda_i v_i(t+T_t)=\lambda_i^2 v_i(t),\\ v_i(t+3T_t)&=\lambda_i v_i(t+2T_t)=\lambda_i^2 v_i(t+T_t)=\lambda_i^3 v_i(t),\\ &\vdots\\ v_i(t+nT_t)&=\lambda_i^n v_i(t), \end{aligned} \tag{29}$$

where n is any non-negative integer, $n=0$ being a trivial result.

The stability state is determined by assessing the ratio of the response at n tooth periods in the future relative to that at the time (t_o) of the disturbance $v_i(t_o)$, i.e., from Eq. (29),

$$\frac{v_i(t_o+nT_t)}{v_i(t_o)}=\lambda_i^n. \tag{30}$$

The growth or decay of the right-hand side with increasing n is governed by the absolute value of λ_i; specifically, as $t\to\infty$ (i.e., as $n\to\infty$), $v_i(t)\to 0$ if $|\lambda_i|<1$ and $v_i(t)\to\infty$ if $|\lambda_i|>1$. The stability boundary corresponds to marginal stability where $|\lambda_i|=1$. Of interest is the frequency content of the constant-amplitude response when operating on the stability boundary.

When $|\lambda_i|=1$, λ_i may be either $+1$ or -1. When $\lambda_i=+1$, Eq. (30) holds for all time and any n only if the response period is T_t. When $\lambda_i=-1$, the sign of λ_i^n alternates as n is incremented. Therefore, when $\lambda_i=-1$, the response period must be $2T_t$. Therefore, the only constant-amplitude sustained responses (i.e., those on the added-lobe boundary) that may occur are those with periods of either T_t or $2T_t$. Since $g(t)$ contains harmonics of ω_t, when run through this analysis, each would show a constant-amplitude response containing that harmonic (multiple) of ω_t as

[3]This forward shift in time by T_t should not be confused with the time delay of T_t associated with regeneration since the two are unrelated.

well as one-half of that. In other words, frequencies of $k\omega_t$ *and* $k\omega_t/2$, $k>0$, the latter encompassing the former, may be present on the added-lobe boundary.

References

[1] Tlusty, J., 1986, "Dynamics of High-Speed Milling," ASME J. Manuf. Sci. Eng., **108**, pp. 59–67.

[2] Merritt, H. E., 1965, "Theory of Self-Excited Machine-Tool Chatter: Contribution to Machine-Tool Chatter Research—1," ASME J. Manuf. Sci. Eng., **87**, pp. 447–454.

[3] Tlusty, J., and Polacek, M., 1963, "The Stability of the Machine Tool Against Self-Excited Vibrations in Machining," *ASME Prod. Engg. Res. Conf.*, Pittsburgh, pp. 454–465.

[4] Nigm, M. M., 1981, "A Method for the Analysis of Machine Tool Chatter," Int. J. Mach. Tool Des. Res., **21**, pp. 251–261.

[5] Budak, E., and Altintas, Y., 1998, "Analytical Prediction of Chatter Stability in Milling—Part I: General Formulation," ASME J. Dyn. Syst., Meas., Control, **120**, pp. 22–30.

[6] Lee, A. C., and Liu, C. S., 1991, "Analysis of Chatter Vibration in the End Milling Processes," Int. J. Mach. Tools Manuf., **31**, pp. 471–479.

[7] Zhang, H., Ni, J., and Shi, H., 1995, "Phase Difference and its Sensitivity Analysis for a Nonlinear Difference-Differential Machining Chatter Model," Trans. NAMRI/SME, **23**, pp. 131–136.

[8] Endres, W. J., 1996, "A Quantitative Energy-Based Method for Predicting Stability Limit as a Direct Function of Spindle Speed for High Speed Machining," Trans. NAMRI/SME, **24**, pp. 27–32.

[9] Olgac, N., and Hosek, M., 1998, "A New Perspective and Analysis for Regenerative Machine Tool Chatter," Int. J. Mach. Tools Manuf., **38**, pp. 783–798.

[10] Sridhar, R., Hohn, R. E., and Long, G. W., 1968, "A General Formulation of the Milling Process Equation—Contribution to Machine Tool Chatter Research—5," ASME J. Ind., **90**, pp. 317–324.

[11] Sridhar, R., Hohn, R. E., and Long, G. W., 1968, "A Stability Algorithm for the General Milling Process—Contribution to Machine Tool Chatter Research—7," ASME J. Ind., **90**, pp. 330–334.

[12] Smith, S., and Tlusty, J., 1991, "An Overview of Modeling and Simulation of Milling Processes," ASME J. Manuf. Sci. Eng., **113**, p. 169.

[13] Minis, I., and Yanushevsky, R., 1993, "A New Theoretical Approach for the Prediction of Machine Tool Chatter in Milling," ASME J. Manuf. Sci. Eng., **115**, pp. 1–8.

[14] Davies, M. A., Pratt, J. R., Dutterer, B. S., and Burns, T. J., 2000, "The Stability of Low Radial Immersion Milling," CIRP Ann., **49**, pp. 37–40.

[15] Davies, M. A., Pratt, J. R., Dutterer, B. S., and Burns, T. J., 2002, "Stability Prediction for Low Radial Immersion Machining," ASME J. Manuf. Sci. Eng., **124**, pp. 217–225.

[16] Bayly, P. V., Halley, J. E., Davies, M. A., and Pratt, J. R., 2000, "Stability Analysis of Intermittent Machining With Finite Time in Cut," *Proc., Symp. on Machining Processes*, ASME IMECE, **MED-11**, pp. 989–996.

[17] Insperger, T., and Stépán, G., 2000, "Stability of the Milling Process," Periodica Polytechnica Ser. Mech. Eng., **44**, pp. 47–57.

[18] Corpus, W. T., 2000, "An Added Stability Phenomenon in Machining Processes With Periodic Time Variation," Ph.D. Thesis, University of Michigan, Ann Arbor, MI.

[19] Endres, W. J., and Ozdoganlar, O. B., 2002, "Existence and Effects of Overlap Factors Greater Than Unity and Less Than Zero," J. Manuf. Proc., **4**, pp. 67–76.

[20] Shorr, M. J., and Liang, S. Y., 1996, "Chatter Stability Analysis for End Milling via Convolution Modeling," Int. J. of Adv. Manuf. Tech., **11**, pp. 311–318.

[21] Endres, W. J., 1997, "An Energy-Based Approach Towards Obtaining an Analytical Solution for Chatter Vibration Level," Tech. Papers of NAMRI/SME, **25**, pp. 27–32.

[22] Corpus, W. T., and Endres, W. J., 2000, "A High-Order Solution for the Added Stability Lobes in Intermittent Machining," *Proc., Symp. on Machining Processes*, ASME IMECE, **MED-11**, pp. 871–878.

[23] Nayfey, A. H., and Mook, D. T., 1979, *Nonlinear Oscillations*, John Wiley & Sons.